Effect of electro-sprayed porous electrodes on the performance and stability of water electrolysis

Jong Yoon Lee [a, b, d] *, Hee-Young Park* [c, d]*, Sang Youp Hwang* [a, d]*, Gi Won Lee* [a]*, Gwan Gyu Park* [a]*, Joseph T. Hupp* [b]*, Jong Hyun Jang* *[c] *and Han-Ik Joh* *[a]

[a] Department of Energy Engineering, Konkuk University, 120 Neungdong-ro, Gwangjin-gu, Seoul 05029, Republic of Korea

[b] Department of Chemistry and International Institute for Nanotechnology, Northwestern University, 2145 Sheridan Road, Evanston, Illinois 60208, USA

[c] Center for Hydrogen Fuel Cell Research, Korea Institute of Science and Technology (KIST), Seoul, 02792, Republic of Korea

[d] These authors contributed equally: Jong Yoon Lee, Hee-Young Park, Sang Youp Hwang

[*]Correspondence: Han-Ik Joh (hijoh@konkuk.ac.kr) and Jong Hyun Jang (jhjang@kist.re.kr)

ABSTRACT

The efficiency of proton exchange membrane water electrolysis (PEMWE) is a critical issue in realizing the production of green hydrogen. The coexistence of three phases in the catalyst layer of PEMWE causes the mass transport limitation at the interfaces between them. In particular, the vigorous production of gaseous hydrogen and oxygen derived from liquid water is generated in the form of bubbles that seriously deactivate the membrane-electrode assembly (MEA). In this study, we investigated the effect of porous structure in the electrode on the efficiency of hydrogen production at high current density, which is highly related to the mass transport limitation. A widely used commercial catalyst (IrO_2) were directly coated on the membrane by the electro-spray method. The porous electrodes on the membrane were formed by the charged catalyst particles that repulsed each other due to the electrostatic forces of the particles. Our membrane electrode assembly (MEA) exhibited outstanding electrolysis performances such as 5.3 A cm^{-2} and 3.2 A cm^{-2} at 2.0 V and 1.8 V, respectively, which are the highest values compared with the results published in the current studies. In addition to the porosity, it was confirmed that optimum binder contents positively affect the hydrophobicity and contact resistance of MEA. Through a simple porosity-controlled technique, the performance of PEMWE, in which three phases coexist, can be improved by more than 60 %. Accordingly, we expect that our systematic study on the role of porosity in the electrodes opens a new era to efficiently produce green hydrogen.

KEYWORDS

mass transport limitation; electrolysis; electro-spray deposition; membrane electrode assembly; porous catalyst layer; Proton exchange membrane water electrolysis (PEMWE)

1. Introduction

Water electrolysis is the eco-friendly technique for producing both hydrogen and oxygen, which is considered the only option to realize carbon neutrality if power generated from renewable energy sources, such as wind and solar energy, is supplied to the electrolysis system. Water electrolysis systems can be categorized into three types based on the electrolyzer: Alkaline Water Electrolysis (AWE), Anion Exchange Membrane Water Electrolysis (AEMWE), and Proton Exchange Membrane Water Electrolysis (PEMWE). Considering the efficiency of each system (AWE: 59-70%, AEMWE: 52-67%, PEMWE: 65-82%), PEMWE emerges as the most promising electrolytic cell due to its higher efficiency and potential for further optimization. [1] However, expensive and scarce materials such as platinum (Pt) and iridium oxide (IrO_2) have been used as electrocatalysts, resulting in higher system and hydrogen production costs. In the last 20 years, the prices of Pt and Ir mineral have risen from £10.58/g and £11.11/g to £28.23/g and £58.22/g, respectively. [2] Therefore, it is necessary to maximize the intrinsic performances of the electrocatalysts since green hydrogen with a reasonable price should be produced to open the zero-carbon era.

The performance of membrane electrode assembly (MEA), in which water is converted into hydrogen and oxygen, is closely related to the triple-phase boundary (TPB). [3–9] Since multiphase complex electrochemical reactions occur in the TPB, the optimum composition of the electrode solution should be finely controlled, assuming the same materials are used as the membrane and electrodes. In particular, it is necessary to design an electrode structure with pores rather than a structure in which an electrocatalyst and an ionomer are densely accumulated, leading to minimizing the mass transport limitation of reactants and products for vigorous reaction conditions. [10]

It has been well-known that the ionomer in the TPB provides a highly conductive ionic pathway from anode to cathode and low contact resistance between the electrodes and membrane. However, excess ionomer covers the active surface of the noble metal catalysts, lowering the electrochemical activities. [11] Hence, the interface engineering of the TPB is essential to improve the MEA performance for the electrolysis. Nevertheless, the optimum contents of the ionomer and the catalysts have still been debated because of the sensitive reaction conditions and complex morphology of the catalyst and the TPB. For instance, Li et al. [12] reported that the maximum electrochemical activity of the electrode was achieved with an optimal Nafion ionomer content of 31 wt.% at a loading of 0.40 mg_{pt} cm^2. In contrast, Antolini et al. [13] represent an optimal ionomer content of 41 wt.% for a loading of 0.20 mg_{pt} cm^2. The ionomer content of the latter is 32.3 wt.% higher than that of the former, even though the loading amount of the catalyst was half of the aforementioned study. In addition, some

recent studies have reported conflicting optimal ionomer contents of approximately 35 wt.% [14] and around 15 wt.% [15] for similar catalyst loadings. Furthermore, some studies have suggested that the optimal ionomer content depends on the catalyst loading. [8]

The catalyst layer in the MEA has been typically fabricated by either coating on membrane (CCM) or gas diffusion layer (CCG) methods. It is well-known that the MEAs prepared by the CCM method exhibit lower contact resistance between the catalyst layer and membrane than those prepared by the CCG method due to the direct coating of the interfaces. [55] However, the sensitivity of the membrane to solvents in the catalyst slurry often results in a heterogeneous coating of the layer. Hence, it is necessary to finely control the slurry composition, deposited contents, and deposition area, when preparing the MEAs using the CCM method. Within the electrochemical cell, three phases coexist: solid (membrane), liquid (water), and gases (hydrogen and oxygen). Thus, minimizing the mass transport limitation of reactants and products is also essential for improving the performance of the MEAs. Therefore, it is necessary to design a uniform electrode structure with pores rather than a structure in which an electrocatalyst and an ionomer are densely accumulated.

Electrocatalysts in the PEMWE should be carefully selected in the limited range because of the acidic and electrochemical corrosive environment. Cathodic catalysts usually use Pt nanoparticles on the carbon supports, which inherently provide pathways themselves for the reactants and products due to their original porous structure. On the other hand, anodic catalysts are exposed to a potential above 1.5 V, necessitating the use of unsupported IrO_2

nanoparticles. Consequently, they were usually coated onto the membrane more densely compared to the Pt/C catalysts, leading to mass transport limitation of water and gases at the anodic electrode with low porosity.

In this study, the IrO_2 particles were directly coated on the membrane by the electro-spray method. Electro-spraying creates a more porous structure primarily due to the electrostatic forces acting on the charged particles during deposition. As the charged particles approach the substrate, electrostatic repulsion between similarly charged particles prevents aggregation, leading to a more uniform and dispersed distribution of the catalyst particles. [16–18, 20, 21, 50, 51, 53, 54] The water electrolysis performance of MEA with electro-spray exhibited outstanding electrolysis performances such as 5.3 A cm^{-2} and 3.2 A cm^{-2} at 2.0 V and 1.8 V, respectively, which are the highest values compared with the results published in the current studies. In addition to the porosity, it was confirmed that optimum binder contents positively affect the hydrophobicity and contact resistance of MEA.

2. Experimental section

2.1. Preparation of catalyst slurry

Iridium oxide (IrO_2) and carbon-supported platinum (46.6 wt.% Pt/C) were purchased from Alfa-acer and Tanaka, respectively. Ionomer (Nafion solution, 5 wt.%) and isopropyl alcohol (IPA) were purchased from Merck-Sigma. The catalyst ink for the anode electrode was prepared using a mixture of IrO_2, deionized water (DIW), ionomer, and IPA. The mixture

solution was sonicated in the bath for 90 min. The detailed amount used in the slurry is summarized in Table S1. The amount of ionomer was adjusted to 10 to 25 wt.% according to the ratio of the total slurry for the ionomer, and each sample code was named by the ratio. The cathode ink was prepared using the same procedure, and only the Pt/C was used instead of IrO_2.

2.2. MEA fabrication

The catalyst layers were directly coated on the membrane by electro- and air-spray methods. The electro-spray was carried out using the electrospinning equipment (eS-robot, NanoNC), and the parameters are summarized in Table S2. The Nafion membrane (50μm, N212, Dupont) was put onto the ground substrate, and a polyvinylchloride (PVC) mask which defined an active area (2.0 x 2.0 cm^2) was placed on the membrane. The prepared catalyst slurry was transferred into the syringe, and then sprayed by the voltage applying. The anode electrode was manufactured using the electro-spray technique, and the cathode electrode was manufactured using the air-spray technique with a slurry with an ionomer content of 20 wt.%. The loading amount of anode and cathode catalyst were 1.0 mg cm^{-2} and 0.4 mg_{pt} cm^{-2}, respectively. Electrosprayed MEA samples are abbreviated as ESM, and the numeric code indicates the amount of ionomer applied to each sample. For the control sample, both the anode and the cathode electrode were manufactured using the air-spray method. The slurry with an ionomer content of 20 wt.% was used as the cathode of the control sample. After coating the catalyst on the membrane, gas diffusion layers (GDLs) were put onto the catalyst

layers to fabricate MEA. As GDLs, Ti paper (Bekaert) and carbon paper (SGL carbon) were used for anode and cathode, respectively.

2.3. Characterization

Morphology and thickness of catalyst layers were confirmed by scanning electron microscope (SEM) (S-2500, Hitachi). The porosity of the catalyst coated on the membrane was determined using a mercury porosimeter (Autopore II, Micromeritics). The hydrophobicity of the fabricated catalyst layer was evaluated using a water contact angle measurement (DSA-100, KRUSS).

2.4. Water electrolysis (PEMWE)

Unit cells were assembled with graphite plates featuring a serpentine flow field for the cathode and Pt-coated titanium end plates for the anode. Fuel cell station (CNL) was used for electrolysis tests. In the activation process, distilled water was supplied to the anode at 15 ccm, the cell temperature was 80 ℃, and a constant voltage was applied at the cell voltage of 1.55 V for 30 minutes. The performance evaluation was conducted in the range of 1.35 to 2.0 V and measured at 50 mV s^{-1}. An electrochemical potentiostat (AutoLab) was used for electrochemical impedance spectroscopy (EIS) analysis. The resistance value at 1.6 V was analyzed, and it was measured under amplitude conditions of 18 mV and frequency conditions of 50 kHz to 50 mHz. The long-term durability of PEMWE was assessed through an accelerated stress test (AST) employing the voltage swing method. [19] This test involved maintaining

potentials of 1.45 V and 2.0 V for 30 seconds each, following a square wave protocol over 20,000 cycles, totaling approximately 167 hours. IV polarization curves were recorded every 2,000 cycles to determine the current density plateau throughout the AST duration and to calculate the decay rate.

3. Results and discussion

The structure of the catalyst layer in a MEA is critical for transport of both reactant and product in water electrolysis with a multiphase system. The MEA is usually composed of unsupported IrO_2 nanoparticles and Pt nanoparticles on carbon supports (Pt/C) as the anode and cathode catalysts, respectively. For the MEAs prepared by conventional air-spray, the thickness of the anode is less than that of the cathode as shown in Figure S1, even though the total amount of IrO_2 (1.0 mg cm^{-2}) is higher than the Pt/C (0.4 mg_{pt} cm^{-2}). It could be inferred that densely packed anodic electrodes seriously hinder effective mass transport compared to the cathode. Hence, an electro-spray method was introduced to prepare the anodic electrode with high porosity in this study. Through the electro-spray method, catalytic nanoparticles in the liquid droplet were dispensed and charged on the membrane, preventing the dense accumulation of the nanoparticles due to the electrostatic interaction. [50, 51] The resulting dispersed empty pores between the catalyst agglomerates increase the porosity and enhance the mass transport via an enlarged diffusion pathway as illustrated in Figure 1(a). On the contrary, the nanoparticles were densely accumulated by the conventional air-spray method, leading to the hindrance of mass transport (Figure 1(b)).

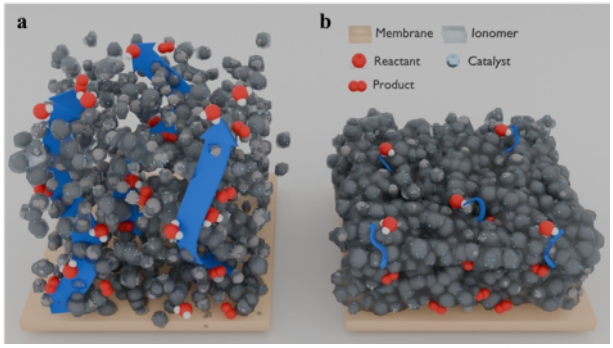

Figure 1. Schematic of catalyst coatings obtained using (a) electro-spray and (b) air-spray method.

Figures 2 and S2 show the SEM images of the cross-section and surface of MEAs fabricated as a function of ionomer contents, respectively, which critically affect the formation of three-phase boundaries. As aforementioned, the catalyst layer formed using the electro-spray was highly dispersed due to the electrostatic interaction and exhibited complex surface roughness (Figure 2 (a) ~ (e)). On the other hand, the MEA manufactured by the air-spray (Figure S2) shows a relatively monotonous and flat surface roughness and very dense catalyst accumulation relative to the electro-sprayed MEAs. The thickness of the catalyst layer containing the same ionomer content (20 wt.%) was measured to be 6.01 ± 0.6 μm for the electro-sprayed layer and 3.61 ± 0.4 μm for the air-sprayed layer, indicating that the electro-spray method increases the catalyst layer thickness by over 60% compared to the air-spray method (Figure 2(f)). These findings align with previous reports by Chaparro et al. [17] and Conde et al. [18], which attributed the formation of a porous structure to the coulombic repulsion among agglomerates of nanoparticles carrying the same charge. The formation of a porous catalyst layer via electro-spraying is governed by coulombic repulsion among charged nanoparticle

agglomerates. [22, 51, 52] As these agglomerates are dispersed in the spraying medium (e.g. Isopropyl alcohol), they acquire a similar charge under the applied electric field. This repulsive interaction prevents their uncontrolled aggregation, leading to a homogeneously distributed catalyst structure. As electro-spraying, the solvent evaporation further intensifies repulsion, ensuring that the catalyst layer remains porous. [17, 18] In contrast, air-sprayed catalyst layers lack this electrostatic effect, resulting in less uniform and dense structures.

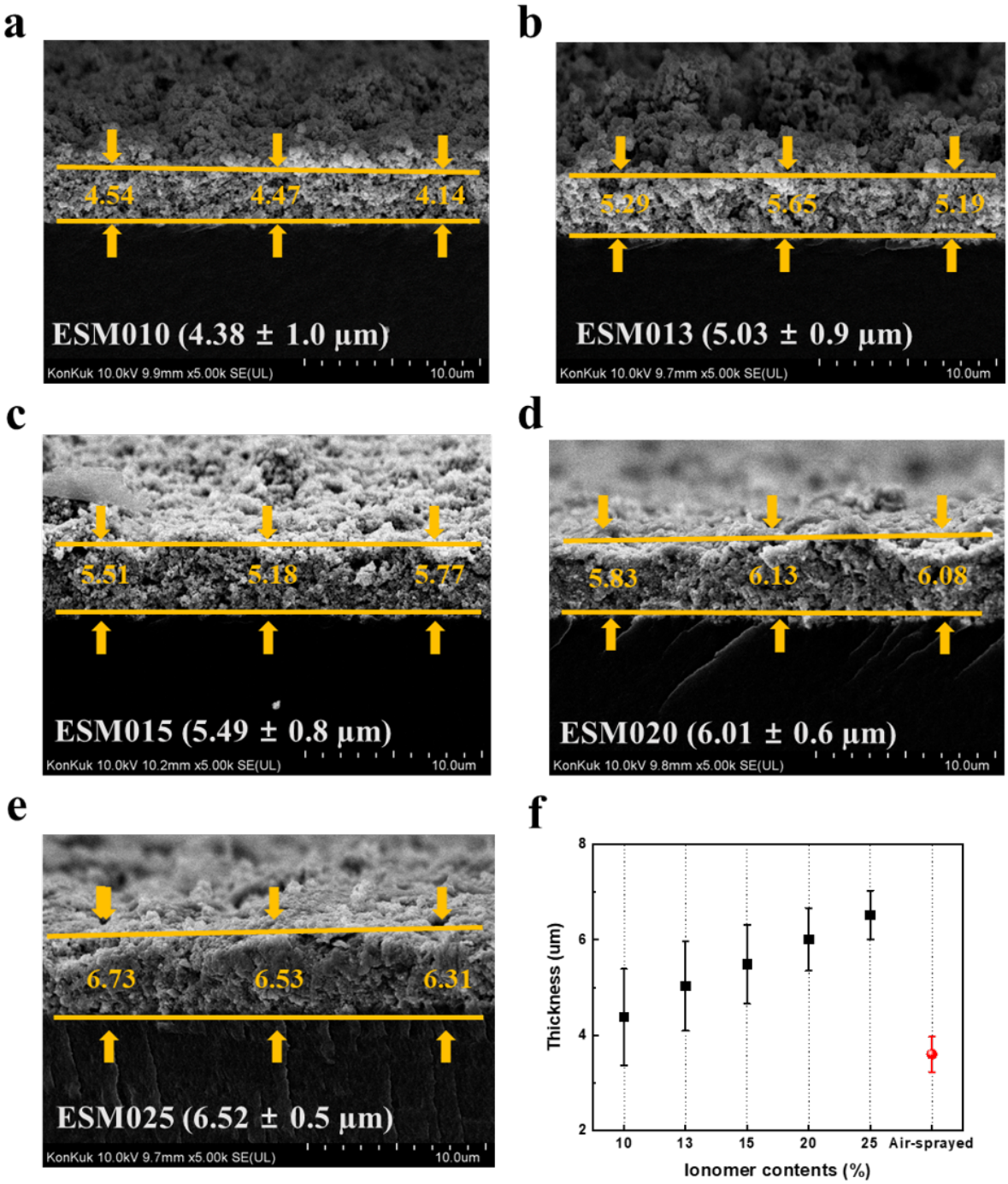

Figure 2. SEM image of MEAs and their measured thickness of catalyst layer on the membrane with different ionomer contents; (a) ~ (e) Cross-section image and (f) Comparison of anode thickness with different ionomer contents using electro- and air-spray methods. Black square and red circle symbols correspond to MEAs constructed using electro- and air-sprays, respectively.

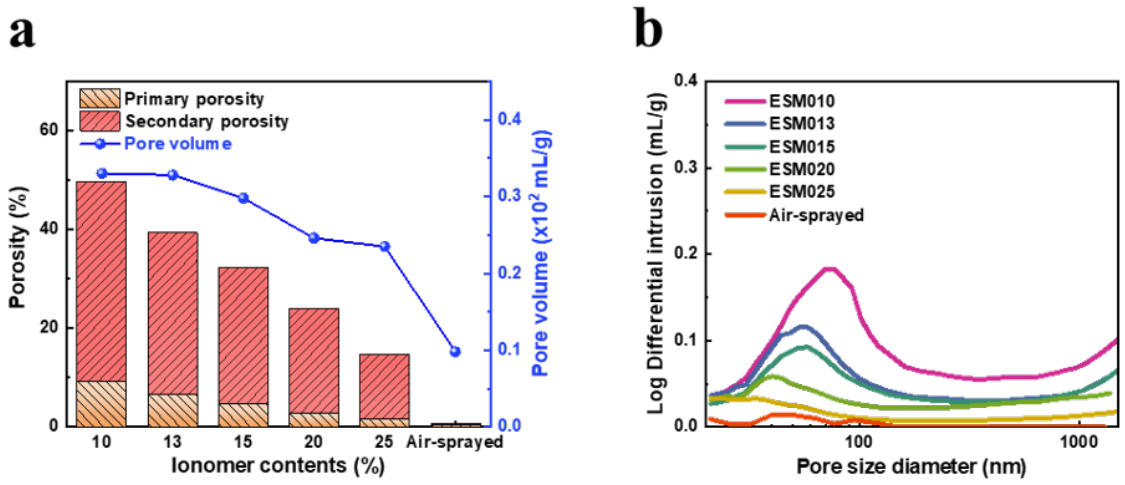

Figure 3. (a) Porosity and pore volume of fabricated MEAs with different ionomer contents and spraying method. (b) Pore size distribution (PSD) of anode electrode with different ionomer contents coated on the membrane using the electro- and the air-spray method.

The effect of the electro-spray method as a function of ionomer content on the porosity at the anode in the MEA was investigated by mercury porosimeter and scanning electron microscopy (SEM) as shown in Figures 3 and S2, respectively. To characterize the properties of catalyst layers in the fabricated MEAs, the porosity and pore volume were compared. The pore volume of the anode remained up to the ionomer content of 15 wt.% and then decreased with the increase of the contents. This finding is consistent with the notion that electrostatic repulsion between electro-sprayed catalytic nanoparticles, is largely responsible for the porosity of the electrode. However, when the ionomer content of the electro-sprayed catalyst layer exceeds 20 wt.%, the ionomer may well cover the pores generated by electro-spray. Hence, the optimum amount of ionomer plays a key role in developing the three-phase interfaces of catalyst, ionomer, and reactant. Interestingly, the PSD results enlarged to a pore

size of less than 1 μm in Figure 3 (b) showed that not only the overall porosity but also the primary and secondary porosity tended to decrease as the ionomer content increased. Primary porosity means smaller pores, usually under 10 nm, that form within agglomerates of carbon particles or catalyst materials. These contribute to the catalyst's surface area and help retain ionomer, which is important for enhancing proton conductivity within the catalyst layer. In contrast, secondary porosity is larger, ranging from 10–50 nm or up to 100 nm, and are located between these particle agglomerates. [59-61] However, a MEA manufactured using the air-spray has a relatively overall tiny porosity. In particular, our electro-sprayed electrode has a well-balanced porosity with primary and secondary pores, which have a ratio of primary to secondary porosity of 0.25 or less. Hao et al. [23] and Ohno et al. [24] suggested that secondary pores in an electrode prepared using only metal nanoparticles with tiny pores might significantly limit the mass transport of reactants and products within the electrode. Moreover, the former reported that the ratio of primary and secondary pores affects the reaction resistance in the electrodes composed of metal nanoparticles. [23] The secondary pores with a size of less than 1.0 μm on the surface of the electro-sprayed electrode can be easily observed by SEM as shown in Figure S2. In addition, we investigated the hydrophobicity of the electrodes by the water contact angle measurement, because the surface of the electrode consisting of charged nanoparticles is rougher than that of the electrode prepared by the conventional air-spray method. As shown in Figure S3 and Table S3, the contact angle values of all samples fabricated by the electro-spray were higher than that by the air-spray. The catalyst layers with the lower ionomer contents (10 – 13%) especially exhibited higher contact angles due to their unique

morphological surface structure [25, 42-44] and hydrophobic properties of ionomer [45-49] (such as Nafion, perfluorosulphonated ionomer (PFSI), Aeminon, Aquivion and hydrocarbon-based polymer electrolyte). Although the ionomer could take up the water, and then be swelled, leading to the lower contact angles, [46, 50] the increased surface roughness and pore structure of the electro-sprayed electrode resulted in a higher contact angle compared to the air-sprayed counterpart when using the same ionomer content (e.g., ESM020). This enhanced hydrophobicity can imply more effective water management within the catalyst layer, facilitating smoother transport of reactants and products to improve electrochemical performance. [56-58]

Figure 4 (a) and (b) present the polarization curves and impedance spectra of MEAs fabricated by electro- and air-spaying. The current densities of electro-sprayed MEAs surpass those of air-sprayed MEAs, particularly at higher voltages of 2.0 V, meaning that extremely vigorous reactions take place. In particular, the current density at 2.0 V for the ESM013 was the best value of about 5.27 A cm^{-2}. This improvement might be attributed to increased porosity, which efficiently enhances diffusive transport of the reactants and products. The relation between porosity and performance based on the current densities at 1.8V and 2.0 V is illustrated in Figure 4 (c). As the porosity of the anode increases, the current density rises linearly. Electrolysis performance of MEAs improved in the following order of ionomer content: 13 > 10 > 15 > 20 > 25 wt.%. This indicates that the excessive ionomer hinders mass transport by covering or filling the pores. The MEA fabricated by the air-spray exhibited the

lowest performance despite having the same catalysts and ionomer content, due to the densely formed catalyst layer.

The electrochemical impedance spectroscopy (EIS) was conducted at a constant voltage (1.6V) and the results are shown in Figure 4 (b). Nyquist plots revealed the internal resistance of electro-sprayed MEAs with the various ionomer contents and air-sprayed MEAs. The intersection points with the Zre axis in the lower frequency range and the size of the semi-circle indicated the ohmic resistance (so-called contact resistance) and charge transfer resistance, respectively. These resistances are also summarized in Table S4. Interestingly, the ohmic resistances at 10 wt.% and 13 wt.%, and the charge transfer resistances at 13 wt.% and 15 wt.% ionomer content, were lower than those of the other samples. The resistances at 13 wt.% ionomer was the lowest overall, resulting in the highest performance for PEMWE. These results suggest that the porosity and internal resistance of MEAs are influenced by ionomer content, which ultimately affects PEMWE performance. [62, 63] An MEA with 10 wt.% ionomer content forms sufficient pores to facilitate electrochemical reactions. However, since the ionomer content in the catalyst layer is insufficient, contact between catalysts is reduced, resulting in higher charge transfer resistance. Conversely, at ionomer contents of 15 wt.% or more, the required electrode loading weight increases, leading to a thicker electrode and higher ohmic resistance. Additionally, at 20 wt.% or more, a few macropores of 50 to 100 nm form, significantly reducing the efficiency of the three-phase interface.

In addition, the EIS analysis of mass transfer resistance was conducted at 1.9 V using an equivalent circuit model comprising one inductor, one resistor, and two resistance–constant phase element (R-CPE) pairs, as detailed in Figure S4 and summarized at Table S5. Based on the fitting results, the resistance R, corresponding to the high-frequency range, was identified as the charge transfer resistance, while the resistance R_1, associated with the low-frequency range, was identified as the mass transfer resistance. [64, 65] The results showed that the R_1 value, representing mass transfer resistance, was 29.1% lower for ESM013 compared to the air-sprayed MEA, indicating improved mass transfer properties. Simultaneously, the charge transfer resistance R was reduced by 14.5% for ESM013 relative to the air-sprayed MEA, suggesting that the optimization of ionomer content enhanced the structural characteristics of the electrode, facilitated gas release, and increased the electrochemically active surface area. Therefore, we believe that an ionomer content of 13 wt.% provides an optimal balance, minimizing both ohmic and charge transfer resistances, and maximizing PEMWE performance by enhancing porosity and three-phase interface efficiency.

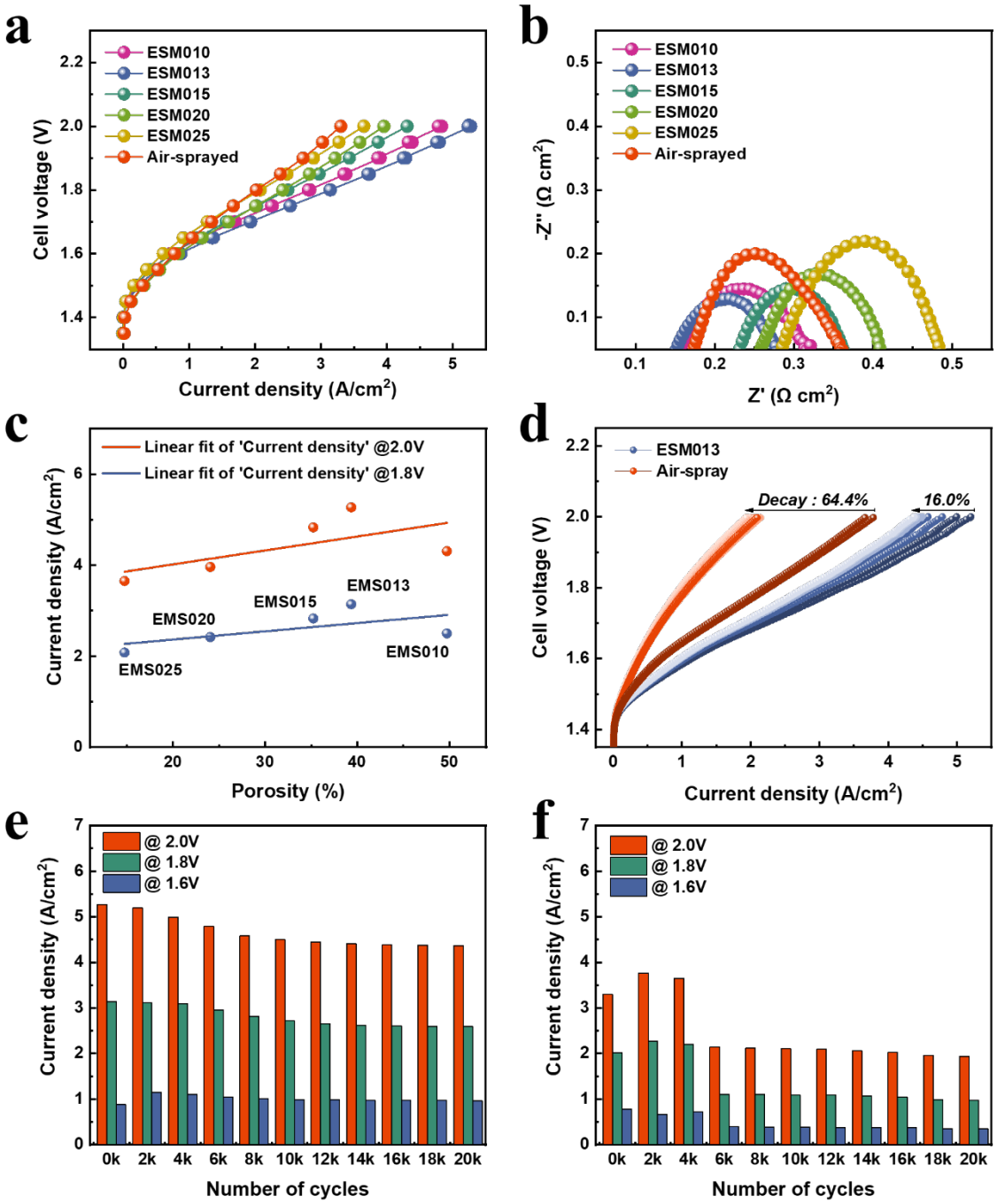

Figure 4. (a) Polarization curves and (b) resistance of the PEMWE single cells with different ionomer contents and spraying method. (c) Linear relation between porosity and performance of PEMWE (red and blue circles referred to current density measured at 2.0 V and 1.8 V, respectively). (d) Polarization curves after AST cycles for spraying method and decay of current density of (e) ESM013 and of (f) Air-sprayed.

Figure 4 (d) ~ (f) presents the AST results for ESM013, which demonstrated the best performance compared to the air-sprayed MEA. ESM013 showed a steady and gradual decrease in current density at 1.8 V and 2.0 V throughout AST cycles, showing a 16.0 % decay from the initial performance at 2.0 V. Interestingly, at 1.6 V, there was a slightly increase in current density after 2k cycles, followed by a gradual decline after 4k cycles (Figure 4 (e)). In contrast, the air-sprayed MEA exhibited an increase in current density after 2k cycles at 1.8 V and 2.0 V but showed a drastic decline after 6k cycles (Figure 4 (f)). These findings suggest that ESM013 likely forms an optimal three-phase boundary due to its appropriate pore structure and hydrophobicity, facilitating efficient reactant transport and product removal. This optimizes targeted electrochemical reactions, especially at high voltage regions like 2.0 V. [26] On the other hand, the air-sprayed MEA seems to suffer from mass transport limitations and resistance, leading to unintended side reactions such as excessive water retention and hindering the removal of oxygen bubbles [26] that significantly impair the durability of the electrochemical catalysts. The MEA exhibited sudden performance degradation after 6,000 cycles, with current density failing to recover in subsequent cycles, culminating in a 64 % decay in performance. The rapid degradation of air-spayed MEAs arises from several factors, stemming from inconsistent catalyst-ionomer distribution and weaker adhesion between the catalyst layer and the membrane. This non-uniform structure results in poor mechanical strength, making the MEAs prone to delamination and structural failure under high operational stress. [25] Additionally, air-sprayed MEAs tend to experience water flooding and gas

bubble accumulation, especially at higher current densities. [26] The limited control over pore size and distribution induces mass transport limitations, leading to localized weak spots and mechanical stress, which accelerate degradation. The poor porosity of air-sprayed MEAs often results in excessive water retention, hindering the removal of oxygen bubbles, which in turn causes the catalyst layer to disintegrate more quickly under sustained high-current operation.

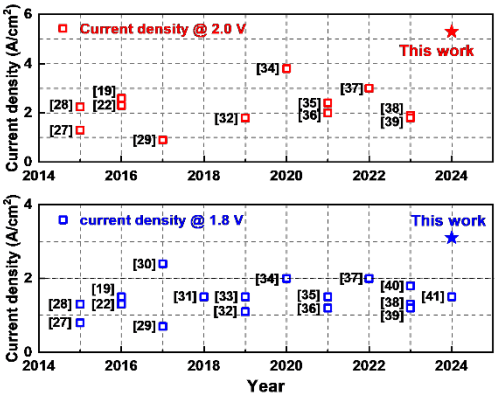

Figure 5. Current density comparison with the results in the previous reports.

Comparison of current densities at 1.8 V and 2.0 V from recently published papers, as depicted in Figure 5, clearly shows that our MEA, prepared via the electro-spray, exhibits outstanding performance (3.1 and 5.3 A cm^{-2} at 1.8 and 2.0 V, respectively) compared to studies evaluating MEAs with commercial IrO_2 catalyst. [19, 22, 27–41] This is particularly notable at high current densities, which fall within the mass transport limitation. Therefore, it can be concluded that the formation of porous electrodes greatly decreases electrical resistance in electrolyzers using our MEAs, contributing to the advancement of cleaner and more environmentally friendly technologies.

4. Conclusions

In this study, we investigate the impact of electrode porous structure, crucial for addressing mass transport limitations, on the efficiency of PEMWE. The MEAs were developed by directly coating the IrO_2 catalyst onto the membrane using an electro-spray method to create the anode electrode. This resulted in exceptional electrolysis performance of 5.3 A cm^{-2} at 2.0 V and 3.2 A cm^{-2} at 1.8 V, representing the highest values compared to those reported in current literature. The influence of ionomer content on MEA porosity, hydrophobicity, and internal resistance was thoroughly examined, revealing that the optimal electrolysis performance was achieved with an ionomer content of 13 wt.%. Porosity control achieved through electro-spraying technology can enhance PEMWE performance by over 60 % in systems where three phases coexist. Consequently, systematic research into electrode porosity and internal resistance is poised to pave the way for efficiently producing green hydrogen in a new era of sustainable energy.

ASSOCIATED CONTENT

Supporting Information

Summary of the catalyst slurry preparation and parameters for the electro-spray deposition; the characterization for the MEAs and electrolysis performance of PEMWEs; Cross-sectional and surface SEM images of coated catalyst on the anode and cathode; Water contact angle comparison; EIS analysis (PDF)

AUTHOR INFORMATION

Corresponding Author

* E-mail: hijoh@konkuk.ac.kr (Han-Ik Joh)

* E-mail: jhjang@kist.re.kr (Jong Hyun Jang)

Present Addresses

[a] Department of Energy Engineering, Konkuk University, 120 Neungdong-ro, Gwangjin-gu, Seoul 05029, Republic of Korea

[b] Department of Chemistry and International Institute for Nanotechnology, Northwestern University, 2145 Sheridan Road, Evanston, Illinois, 60208, USA

[c] Center for Hydrogen Fuel Cell Research, Korea Institute of Science and Technology (KIST), Seoul, 02792, Republic of Korea

Author Contributions

Jong Yoon Lee, Hee-Young Park and Sang Youp Hwang conducted the experiment, analysis and wrote the manuscripts. Gi Won Lee and Gwan Gyu Park performed the analysis and participated in the discussion. Joseph T. Hupp helped supervise the project. Jong Hyun Jang and Han-Ik Joh supervised the whole project.

Notes

The authors declare no competing financial interest.

ACKNOWLEDGMENT

This work was supported by the Korea Institute of Energy Technology Evaluation and Planning (RS-2024-00404073), and National Research Foundation of Korea by the Ministry of Science and ICT (RS-2024-00413272). J.T.H. gratefully acknowledges the U.S. Dept. of Energy, Office of Science, Basic Energy Sciences, Solar Photochemistry Program (DE-FG02-87ER-13808)

REFERENCES

(1) Chen, Y.; Liu, C.; Xu, J.; Xia, C.; Wang, P.; Xia, B. Y.; Yan, Y.; Wang, X. Key Components and Design Strategy for a Proton Exchange Membrane Water Electrolyzer. *Small Struct.* **2023**, *4* (6), 2200130. https://doi.org/10.1002/sstr.202200130

(2) Wang, Y.; Pang, Y.; Xu, H.; Martinez, A.; Chen, K. S. PEM Fuel Cell and Electrolysis Cell Technologies and Hydrogen Infrastructure Development – a Review. *Energy Environ. Sci.* **2022**, *15* (6), 2288–2328. https://doi.org/10.1039/D2EE00790H

(3) Pan, S.; Wen, Q.; Dan, X.; Li, Y.; Ning, F.; He, C.; Li, W.; Shen, M.; He, L.; Tian, B.; Zhang, Y.; Feng, W.; Zou, Y.; Zhou, X. Enhanced Triple-Phase Interface in PEMFC by Proton Conductor Absorption on the Pt Catalyst. *ACS Appl. Energy Mater.* **2023**, *6* (2), 763–772. https://doi.org/10.1021/acsaem.2c02992

(4) Fouzaï, I.; Gentil, S.; Bassetto, V. C.; Silva, W. O.; Maher, R.; Girault, H. H. Catalytic Layer-Membrane Electrode Assembly Methods for Optimum Triple Phase Boundaries and

Fuel Cell Performances. *J. Mater. Chem. A* **2021**, *9* (18), 11096–11123. https://doi.org/10.1039/D0TA07470E

(5) Wang, Y.-C.; Huang, W.; Wan, L.-Y.; Yang, J.; Xie, R.-J.; Zheng, Y.-P.; Tan, Y.-Z.; Wang, Y.-S.; Zaghib, K.; Zheng, L.-R.; Sun, S.-H.; Zhou, Z.-Y.; Sun, S.-G. Identification of the Active Triple-Phase Boundary of a Non-Pt Catalyst Layer in Fuel Cells. *Sci. Adv.* **2022**, *8* (44), eadd8873. https://doi.org/10.1126/sciadv.add8873

(6) Dao, D. Van; Adilbish, G.; Le, T. D.; Lee, I.-H.; Yu, Y.-T. Triple Phase Boundary and Power Density Enhancement in PEMFCs of a Pt/C Electrode with Double Catalyst Layers. *RSC Adv.* **2019**, *9* (27), 15635–15641. https://doi.org/10.1039/C9RA01741K

(7) Karuppanan, K. K.; Raghu, A. V.; Panthalingal, M. K.; Ramanathan, S.; Kumaresan, T.; Pullithadathil, B. Triple Phase Boundary Augmentation in Hierarchical, Pt Grafted N-Doped Mesoporous Carbon Nanofibers for High Performance and Durable PEM Fuel Cells. *J. Mater. Chem. A* **2018**, *6* (26), 12768–12781. https://doi.org/10.1039/C8TA02391C

(8) Sasikumar, G.; Ihm, J. W.; Ryu, H. Dependence of Optimum Nafion Content in Catalyst Layer on Platinum Loading. *J. Power Sources* **2004**, *132* (1), 11–17. https://doi.org/10.1016/j.jpowsour.2003.12.060

(9) Afsahi, F.; Mathieu-Potvin, F.; Kaliaguine, S. Impact of Ionomer Content on Proton Exchange Membrane Fuel Cell Performance. *Fuel Cells* **2016**, *16* (1), 107–125. https://doi.org/10.1002/fuce.201500138

(10) Doo, G.; Lee, J. H.; Yuk, S.; Choi, S.; Lee, D.-H.; Lee, D. W.; Kim, H. G.; Kwon, S. H.; Lee, S. G.; Kim, H.-T. Tuning the Ionomer Distribution in the Fuel Cell Catalyst Layer with Scaling the Ionomer Aggregate Size in Dispersion. *ACS Appl. Mater. Interfaces* **2018**, *10* (21), 17835–17841. https://doi.org/10.1021/acsami.8b01751

(11) Chiriaev, S.; Madsen, N. D.; Rubahn, H.-G.; Andersen, S. M. Helium Ion Microscopy of Proton Exchange Membrane Fuel Cell Electrode Structures. *AIMS Mater. Sci.* **2017**, *4* (6), 1289–1304. https://doi.org/10.3934/matersci.2017.6.1289

(12) Li, G.; Pickup, P. G. Ionic Conductivity of PEMFC Electrodes : Effect of Nafion Loading. *J. Electrochem. Soc.* **2003**, *150* (11), C745. https://doi.org/10.1149/1.1611493

(13) Antolini, E.; Giorgi, L.; Pozio, A.; Passalacqua, E. Influence of Nafion Loading in the Catalyst Layer of Gas-Diffusion Electrodes for PEFC. *J. Power Sources* **1999**, *77* (2), 136–142. https://doi.org/10.1016/S0378-7753(98)00186-4

(14) Viva, F. A.; Bruno, M. M.; Franceschini, E. A.; Thomas, Y. R. J.; Ramos Sanchez, G.; Solorza-Feria, O.; Corti, H. R. Mesoporous Carbon as Pt Support for PEM Fuel Cell. *Int. J. Hydrogen Energy* **2014**, *39* (16), 8821–8826. https://doi.org/10.1016/j.ijhydene.2013.12.027

(15) Chaparro, A. M.; Gallardo, B.; Folgado, M. A.; Martín, A. J.; Daza, L. PEMFC Electrode Preparation by Electrospray: Optimization of Catalyst Load and Ionomer Content. *Catal. Today* **2009**, *143* (3), 237–241. https://doi.org/10.1016/j.cattod.2008.12.003

(16) Ferreira-Aparicio, P.; Chaparro, A. M.; Folgado, M. A.; Conde, J. J.; Brightman, E.; Hinds, G. Degradation Study by Start-Up/Shut-Down Cycling of Superhydrophobic Electrosprayed Catalyst Layers Using a Localized Reference Electrode Technique. *ACS Appl. Mater. Interfaces* **2017**, *9* (12), 10626–10636. https://doi.org/10.1021/acsami.6b15581

(17) Chaparro, A. M.; Folgado, M. A.; Ferreira-Aparicio, P.; Martín, A. J.; Alonso-Álvarez, I.; Daza, L. Properties of Catalyst Layers for PEMFC Electrodes Prepared by Electrospray Deposition. *J. Electrochem. Soc.* **2010**, *157* (7), B993. https://doi.org/10.1149/1.3425740

(18) Conde, J. J.; Ferreira-Aparicio, P.; Chaparro, A. M. Anti-Corrosion Coating for Metal Surfaces Based on Superhydrophobic Electrosprayed Carbon Layers. *Appl. Mater. Today* **2018**, *13*, 100–106. https://doi.org/10.1016/j.apmt.2018.08.001

(19) Alia, S. M.; Rasimick, B.; Ngo, C.; Neyerlin, K. C.; Kocha, S. S.; Pylypenko, S.; Xu, H.; Pivovar, B. S. Activity and Durability of Iridium Nanoparticles in the Oxygen Evolution Reaction. *J. Electrochem. Soc.* **2016**, *163* (11), F3105. https://doi.org/10.1149/2.0151611jes

(20) Collins, R. T.; Jones, J. J.; Harris, M. T.; Basaran, O. A. Electrohydrodynamic Tip Streaming and Emission of Charged Drops from Liquid Cones. *Nat. Phys.* **2008**, *4* (2), 149–154. https://doi.org/10.1038/nphys807

(21) Kostiainen, R.; Kauppila, T. J. Effect of Eluent on the Ionization Process in Liquid Chromatography–Mass Spectrometry. *J. Chromatogr. A* **2009**, *1216* (4), 685–699. https://doi.org/10.1016/j.chroma.2008.08.095

(22) Rozain, C.; Mayousse, E.; Guillet, N.; Millet, P. Influence of Iridium Oxide Loadings on the Performance of PEM Water Electrolysis Cells: Part II – Advanced Oxygen Electrodes. *Appl. Catal. B* **2016**, *182*, 123–131. https://doi.org/10.1016/j.apcatb.2015.09.011

(23) Hao, M.; Assresahegn, B. D.; Abdellah, A.; Miner, L.; Al Hejami, A.; Zaker, N.; Gaudet, J.; Roué, L.; Botton, G. A.; Beauchemin, D.; Higgins, D. C.; Thorpe, S.; Harrington, D. A.; Guay, D. Role of Ir Decoration in Activating a Multiscale Fractal Surface in Porous Ni for the Oxygen Evolution Reaction. *ACS Catal.* **2023**, *13* (3), 1726–1739. https://doi.org/10.1021/acscatal.2c05349

(24) Ohno, H.; Nohara, S.; Kakinuma, K.; Uchida, M.; Uchida, H. Effect of Electronic Conductivities of Iridium Oxide/Doped SnO2 Oxygen-Evolving Catalysts on the Polarization Properties in Proton Exchange Membrane Water Electrolysis. *Catalysts* **2019**, *9* (1). https://doi.org/10.3390/catal9010074

(25) Kim, S. H.; Lee, G. C.; Kang, J. Y.; Moriyama, K.; Park, H. S.; Kim, M. H. The Role of Surface Energy in Heterogeneous Bubble Growth on Ideal Surface. *Int. J. Heat Mass Transf.* **2017**, *108*, 1901–1909. https://doi.org/10.1016/j.ijheatmasstransfer.2016.10.005

(26) Yuan, S.; Zhao, C.; Cai, X.; An, L.; Shen, S.; Yan, X.; Zhang, J. Bubble Evolution and Transport in PEM Water Electrolysis: Mechanism, Impact, and Management. *Prog. Energy Combust. Sci.* **2023**, *96*, 101075. https://doi.org/10.1016/j.pecs.2023.101075

(27) Oh, H.-S.; Nong, H. N.; Reier, T.; Gliech, M.; Strasser, P. Oxide-Supported Ir Nanodendrites with High Activity and Durability for the Oxygen Evolution Reaction in Acid PEM Water Electrolyzers. *Chem. Sci.* **2015**, *6* (6), 3321–3328. https://doi.org/10.1039/C5SC00518C

(28) Lee, B.-S.; Ahn, S. H.; Park, H.-Y.; Choi, I.; Yoo, S. J.; Kim, H.-J.; Henkensmeier, D.; Kim, J. Y.; Park, S.; Nam, S. W.; Lee, K.-Y.; Jang, J. H. Development of Electrodeposited IrO_2 Electrodes as Anodes in Polymer Electrolyte Membrane Water Electrolysis. *Appl Catal. B* **2015**, *179*, 285–291. https://doi.org/10.1016/j.apcatb.2015.05.027

(29) Lim, J.; Park, D.; Jeon, S. S.; Roh, C.-W.; Choi, J.; Yoon, D.; Park, M.; Jung, H.; Lee, H. Ultrathin IrO_2 Nanoneedles for Electrochemical Water Oxidation. *Adv. Funct. Mater.* **2018**, *28* (4), 1704796. https://doi.org/10.1002/adfm.201704796

(30) Siracusano, S.; Hodnik, N.; Jovanovic, P.; Ruiz-Zepeda, F.; Šala, M.; Baglio, V.; Aricò, A. S. New Insights into the Stability of a High performance Nanostructured Catalyst for Sustainable Water Electrolysis. *Nano Energy* **2017**, *40*, 618–632. https://doi.org/10.1016/j.nanoen.2017.09.014

(31) Kang, Z.; Yang, G.; Mo, J.; Yu, S.; Cullen, D. A.; Retterer, S. T.; Toops, T. J.; Brady, M. P.; Bender, G.; Pivovar, B. S.; Green, J. B.; Zhang, F.-Y. Developing Titanium Micro/Nano Porous Layers on Planar Thin/Tunable LGDLs for High-Efficiency Hydrogen Production.

Int. J. Hydrogen Energy **2018**, *43* (31), 14618–14628. https://doi.org/10.1016/j.ijhydene.2018.05.139

(32) Park, J. E.; Kang, S. Y.; Oh, S.-H.; Kim, J. K.; Lim, M. S.; Ahn, C.-Y.; Cho, Y.-H.; Sung, Y.-E. High-Performance Anion-Exchange Membrane Water Electrolysis. *Electrochim. Acta* **2019**, *295*, 99–106. https://doi.org/10.1016/j.electacta.2018.10.143

(33) Kang, Z.; Yu, S.; Yang, G.; Li, Y.; Bender, G.; Pivovar, B. S.; Green, J. B.; Zhang, F.-Y. Performance Improvement of Proton Exchange Membrane Electrolyzer Cells by Introducing In-Plane Transport Enhancement Layers. *Electrochim. Acta* **2019**, *316*, 43–51. https://doi.org/10.1016/j.electacta.2019.05.096

(34) Pham, C. Van; Bühler, M.; Knöppel, J.; Bierling, M.; Seeberger, D.; Escalera-López, D.; Mayrhofer, K. J. J.; Cherevko, S.; Thiele, S. IrO_2 Coated TiO2 Core-Shell Microparticles Advance Performance of Low Loading Proton Exchange Membrane Water Electrolyzers. *Appl. Catal. B* **2020**, *269*, 118762. https://doi.org/10.1016/j.apcatb.2020.118762

(35) Huang, H.; Kim, H.; Lee, A.; Kim, S.; Lim, W.-G.; Park, C.-Y.; Kim, S.; Kim, S.-K.; Lee, J. Structure Engineering Defective and Mass Transfer-Enhanced RuO2 Nanosheets for Proton Exchange Membrane Water Electrolyzer. *Nano Energy* **2021**, *88*, 106276. https://doi.org/10.1016/j.nanoen.2021.106276

(36) Jiang, G.; Yu, H.; Li, Y.; Yao, D.; Chi, J.; Sun, S.; Shao, Z. Low-Loading and Highly Stable Membrane Electrode Based on an Ir@WOxNR Ordered Array for PEM Water

Electrolysis. *ACS Appl. Mater. Interfaces* **2021**, *13* (13), 15073–15082. https://doi.org/10.1021/acsami.0c20791

(37) Lim, J.; Kang, G.; Lee, J. W.; Jeon, S. S.; Jeon, H.; Kang, P. W.; Lee, H. Amorphous Ir Atomic Clusters Anchored on Crystalline IrO_2 Nanoneedles for Proton Exchange Membrane Water Oxidation. *J. Power Sources* **2022**, *524*, 231069. https://doi.org/10.1016/j.jpowsour.2022.231069

(38) Lee, C.; Shin, K.; Park, Y.; Yun, Y. H.; Doo, G.; Jung, G. H.; Kim, M.; Cho, W.-C.; Kim, C.-H.; Lee, H. M.; Kim, H. Y.; Lee, S.; Henkelman, G.; Cho, H.-S. Catalyst-Support Interactions in Zr2ON2-Supported IrOx Electrocatalysts to Break the Trade-Off Relationship Between the Activity and Stability in the Acidic Oxygen Evolution Reaction. *Adv. Funct. Mater* **2023**, *33* (25), 2301557. https://doi.org/10.1002/adfm.202301557

(39) Wang, Y.; Zhang, M.; Kang, Z.; Shi, L.; Shen, Y.; Tian, B.; Zou, Y.; Chen, H.; Zou, X. Nano-Metal Diborides-Supported Anode Catalyst with Strongly Coupled TaOx/IrO_2 Catalytic Layer for Low-Iridium-Loading Proton Exchange Membrane Electrolyzer. *Nat. Commun.* **2023**, *14* (1), 5119. https://doi.org/10.1038/s41467-023-40912-8

(40) Duan, X.; Liu, H.; Zhang, W.; Ma, Q.; Xu, Q.; Khotseng, L.; Su, H. Boosting the Efficiency of IrOx Nanoparticles with Micron-Flower Nb4N5 Support for Oxygen Evolution Reaction in Polymer Electrolyte Membrane Water Electrolyzer. *Electrochim. Acta* **2023**, *470*, 143271. https://doi.org/10.1016/j.electacta.2023.143271

(41) Xie, Z.; Ding, L.; Yu, S.; Wang, W.; Capuano, C. B.; Keane, A.; Ayers, K.; Cullen, D. A.; Meyer, H. M.; Zhang, F.-Y. Ionomer-Free Nanoporous Iridium Nanosheet Electrodes with Boosted Performance and Catalyst Utilization for High-Efficiency Water Electrolyzers. *Appl. Catal. B* **2024**, *341*, 123298. https://doi.org/10.1016/j.apcatb.2023.123298

(42) Zhang, W.; Huang, H.; Wen, F.; Ren, L.; Ning, Z.; Jia, Z.; Cheng, Z.; Lyu, F. Insights into the Relationship between Wettability and Surface Roughness in Tight Reservoirs from a Pore-Scale View: Effect of Electric Field. *Energy & Fuels* **2023**, *37* (8), 5867–5877. https://doi.org/10.1021/acs.energyfuels.3c00406

(43) Pandey, P. R.; Roy, S. Is It Possible to Change Wettability of Hydrophilic Surface by Changing Its Roughness? *J. Phys. Chem. Lett.* **2013**, *4* (21), 3692–3697. https://doi.org/10.1021/jz401946v

(44) Yamada, Y.; Murase, M.; Yatsugi, K.; Mizoshita, N. Laser Desorption/Ionization Mass Spectrometry Using TiO2 Nanopillar Array Substrates with Tunable Surface Roughness and Wettability. *ACS Appl. Nano Mater.* **2021**, *4* (12), 13884–13895. https://doi.org/10.1021/acsanm.1c03222

(45) Conde, J. J.; Chaparro, A. M.; Ferreira-Aparicio, P. Understanding the Behavior of Electrosprayed Carbon Black-Nafion Composite Layers. *Fuel Cells* **2018**, *18* (5), 627–639. https://doi.org/10.1002/fuce.201700218

(46) Gebel, G. Structural Evolution of Water Swollen Perfluorosulfonated Ionomers from Dry Membrane to Solution. *Polymer (Guildf)* **2000**, *41* (15), 5829–5838. https://doi.org/10.1016/S0032-3861(99)00770-3

(47) Koch, S.; Heizmann, P. A.; Kilian, S. K.; Britton, B.; Holdcroft, S.; Breitwieser, M.; Vierrath, S. The Effect of Ionomer Content in Catalyst Layers in Anion-Exchange Membrane Water Electrolyzers Prepared with Reinforced Membranes (Aemion+TM). *J. Mater. Chem. A* **2021**, *9* (28), 15744–15754. https://doi.org/10.1039/D1TA01861B

(48) Gatto, I.; Saccà, A.; Sebastián, D.; Baglio, V.; Aricò, A. S.; Oldani, C.; Merlo, L.; Carbone, A. Influence of Ionomer Content in the Catalytic Layer of MEAs Based on Aquivion® Ionomer. *Polymers (Basel)* **2021**, *13* (21). https://doi.org/10.3390/polym13213832

(49) Nguyen, H.; Sultanova, D.; Heizmann, P. A.; Vierrath, S.; Breitwieser, M. Improving the Efficiency of Fully Hydrocarbon-Based Proton-Exchange Membrane Fuel Cells by Ionomer Content Gradients in Cathode Catalyst Layers. *Mater. Adv.* **2022**, *3* (23), 8460–8468. https://doi.org/10.1039/D2MA00761D

(50) Shi, C.; Liu, T.; Chen, W.; Cui, F.; Liu, L.; Cai, Y.; Li, Y. Interaction, Structure and Tensile Property of Swollen Nafion® Membranes. *Polymer (Guildf)* **2021**, *213*, 123224. https://doi.org/10.1016/j.polymer.2020.123224

(51) Arai, H.; Asami, K.; Ito, H.; Katayama, N. Effect of the Settings of Electrospray Deposition Method on the Structure and Performance of the Fuel Cell Catalyst Layer. *Current Applied Physics* **2022**, *39*, 296–303. https://doi.org/10.1016/j.cap.2022.05.014

(52) Conde, J. J.; Ferreira-Aparicio, P.; Chaparro, A. M. Electrospray Deposition: A Breakthrough Technique for Proton Exchange Membrane Fuel Cell Catalyst Layer Fabrication. *ACS Appl. Energy Mater* **2021**, *4* (8), 7394–7404. https://doi.org/10.1021/acsaem.1c01445

(53) Jaworek, A. Micro- and Nanoparticle Production by Electrospraying. *Powder Technol* **2007**, *176* (1), 18–35. https://doi.org/10.1016/j.powtec.2007.01.035

(54) Loscertales, I. G.; Barrero, A.; Guerrero, I.; Cortijo, R.; Marquez, M.; Gañán-Calvo, A. M. Micro/Nano Encapsulation via Electrified Coaxial Liquid Jets. *Science (1979)* **2002**, *295* (5560), 1695–1698. https://doi.org/10.1126/science.1067595

(55) Vinodh, R.; Palanivel, T.; Kalanur, S. S.; Pollet, B. G. Recent Advancements in Catalyst Coated Membranes for Water Electrolysis: A Critical Review. *Energy Advances* **2024**, *3* (6), 1144–1166. https://doi.org/10.1039/D4YA00143E

(56) Li, A.; Han, M.; Chan, S. H.; Nguyen, N. Effects of Hydrophobicity of the Cathode Catalyst Layer on the Performance of a PEM Fuel Cell. *Electrochim Acta* **2010**, *55* (8), 2706–2711. https://doi.org/https://doi.org/10.1016/j.electacta.2009.12.048

(57) Avcioglu, G. S.; Ficicilar, B.; Eroglu, I. Improved PEM Fuel Cell Performance with Hydrophobic Catalyst Layers. *Int J Hydrogen Energy* **2018**, *43* (40), 18632–18641. https://doi.org/https://doi.org/10.1016/j.ijhydene.2018.03.045

(58) Ma, J.; Ma, H.; Lin, J.; Zhang, Y.; Xiao, L.; Zhuang, L.; Xu, P.; Chen, L. Hydrophobic Modification Enhances the Microstructure Stability of the Catalyst Layer in Alkaline Polymer Electrolyte Fuel Cells. *RSC Adv* **2024**, *14* (37), 26738–26746. https://doi.org/10.1039/D4RA04019H.

(59) Malekian, A.; Salari, S.; Stumper, J.; Djilali, N.; Bahrami, M. Effect of Compression on Pore Size Distribution and Porosity of PEM Fuel Cell Catalyst Layers. *Int J Hydrogen Energy* **2019**, *44* (41), 23396–23405. https://doi.org/10.1016/j.ijhydene.2019.07.036

(60) Tang, H.; Geng, K.; Aili, D.; Ju, Q.; Pan, J.; Chao, G.; Yin, X.; Guo, X.; Li, Q.; Li, N. Low Pt Loading for High-Performance Fuel Cell Electrodes Enabled by Hydrogen-Bonding Microporous Polymer Binders. *Nat Commun* **2022**, *13* (1), 7577. https://doi.org/10.1038/s41467-022-34489-x

(61) Ni, Z.; Wang, L.; Wang, B. Unveiling the Impact of Pore Structure of Cathode Catalyst Layer on Proton Exchange Membrane Cell Performance. *Int J Hydrogen Energy* **2024**, *60*, 1404–1413. https://doi.org/10.1016/j.ijhydene.2024.02.303

(62) Volk, E. K.; Kreider, M. E.; Kwon, S.; Alia, S. M. Recent Progress in Understanding the Catalyst Layer in Anion Exchange Membrane Electrolyzers – Durability, Utilization, and Integration. *EES Catalysis* **2024**, *2* (1), 109–137. https://doi.org/10.1039/D3EY00193H

(63) Cheng, F.; Tian, T.; Wang, R.; Zhang, H.; Zhu, L.; Tang, H. Structure–Performance Correlation Inspired Platinum-Assisted Anode with a Homogeneous Ionomer Layer for Proton Exchange Membrane Water Electrolysis. *Polymers (Basel)* **2024**, *16* (2). https://doi.org/10.3390/polym16020237

(64) Ramesh K. S., Ruttala D., Tathagata K., Arup C. and Manoj N., Electrochemical Impedance Spectroscopy of Oxygen Reduction Reaction (ORR) in a Rotating Disk Electrode Configuration: Effect of Ionomer Content and Carbon-Support, *J. Electrochem. Soc.,* **2015**, 162(6). https://doi.org/10.1149/2.0141506jes

(65) Miji E. J., Anand K. T., Divya P., Debittree C., Manoj N., What contributes to the internal mass-transport resistance of redox species through porous thin-film electrodes?, Phys. Chem. Chem. Phys., **2022**, 24, 3886-3895. https://doi.org/10.1039/D1CP05107E

Table of Contents (TOC) Graphic